Quantum Dot Behavior in Bilayer Graphene Nanoribbons

Minsheng Wang,[†,§] Emil B. Song,[†,§] Sejoon Lee,[†,‡,*] Jianshi Tang,[†] Murong Lang,[†] Caifu Zeng,[†] Guangyu Xu,[†] Yi Zhou,[†] and Kang L. Wang[†,*]

[†]Department of Electrical Engineering, University of California at Los Angeles, Los Angeles, California 90095, United States and, [‡]Quantum-Functional Semiconductor Research Center, Dongguk University-Seoul, Seoul 100-715, Korea. [§]These authors contributed equally to this work.

ABSTRACT

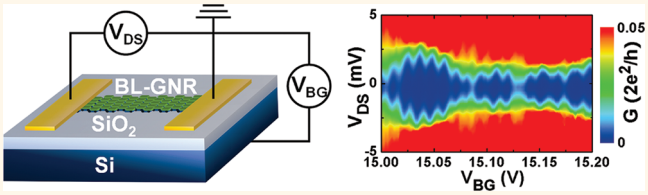

Bilayer graphene has recently earned great attention for its unique electronic properties and commendable use in electronic applications. Here, we report the observation of quantum dot (QD) behaviors in bilayer graphene nanoribbons (BL-GNRs). The periodic Coulomb oscillations indicate the formation of a single quantum dot within the BL-GNR because of the broad distribution function of the carrier concentration fluctuation at the charge neutrality point. The size of the QD changes as we modulate the relative position between the Fermi level and surface potential. Furthermore, the potential barriers forming the QD remain stable at elevated temperatures and external bias. In combination with the observation of transport gaps, our results suggest that the disordered surface potential creates QDs along the ribbon and governs the electronic transport properties in BL-GNRs.

KEYWORDS: bilayer graphene · nanoribbon · quantum dot · Coulomb blockade oscillation

Since its first appearance in 2004,[1] graphene has attracted enormous research activities because of its unique physical and electronic properties. From the perspective of electronic applications, efforts have been made to create an energy band gap in this otherwise gapless material, among which graphene nanoribbon (GNR) is one of the most extensively explored systems.[2−5] To date, studies on GNRs have been focused on single-layer graphene nanoribbons (SL-GNRs), which have surmounted in the observation of the electronic energy sub-bands through quantum confinement,[6,7] the transport gap induced by disorders,[8] and the Coulomb blockade effect from electron−hole puddles and/or edge roughness.[9,10] In comparison to single-layer graphene, bilayer graphene has its unique electronic properties, such as the parabolic band structure,[11] the electric-field-induced band gap,[12−14] and the distinctive Klein tunneling behavior,[15] which all can alter the transport properties of GNRs and be exploited for device applications. According to recent theoretical studies, bilayer GNRs (BL-GNRs) are predicted to exhibit strong optical responses in the terahertz regime[16,17] and tunable magnetic properties[18−21] for photonics and spintronics applications. Therefore, it is important to understand the fundamental electronic transport properties of BL-GNRs. In this paper, we study the transport behaviors of etched BL-GNRs fabricated using nanowire masks (see Materials and Methods).

RESULTS AND DISCUSSION

In order to understand the overall transport behavior of the BL-GNR (Figure 1a,b), we first investigate the conductance dependence throughout a wide range of gate (V_{BG}) and source-drain voltages (V_{DS}) using a standard low-frequency lock-in technique (Figure 1c). As shown in the inset of Figure 2a, the conductance of the BL-GNR is strongly suppressed near the charge neutrality point with repeatable resonance peaks depicting gap-like behaviors. It has been predicted that the quantum confinement energy gaps of BL-GNRs are less than those of SL-GNRs for a given width because of the interlayer coupling.[18] Accordingly, as shown in Table 1, the confinement gap of our 50 nm wide BL-GNR is expected to be <6.6 meV (of SL-GNR with 50 nm width),[22] while the electric-field-induced energy gap is estimated to be ∼2 meV at 0.02 V/nm ($V_{BG} - V_{Dirac} \approx 5$ V).[14] However, we observe a gap of $\Delta E_F = 87$ meV near $V_{DS} \approx 0$ V. This gap can be calculated using $\Delta E_F = \hat{C}_{BG}\Delta V_{BG}\pi\hbar^2/2m^*e$, where m^* (=0.054 m_e)[11] is the effective mass, ΔV_{BG} (=6 V) is the voltage range of the gap (Figure 2a), and $\hat{C}_{BG}$ (=1.04 × 10^{-21} F/nm^2) is the capacitance per unit area that takes into account the fringing effect.[6,23] Here, ΔE_F is greater than both the quantum confinement energy

* Address correspondence to sejoon@ee.ucla.edu, wang@ee.ucla.edu.

Received for review July 21, 2011 and accepted October 23, 2011.

Published online October 23, 2011
10.1021/nn2027566

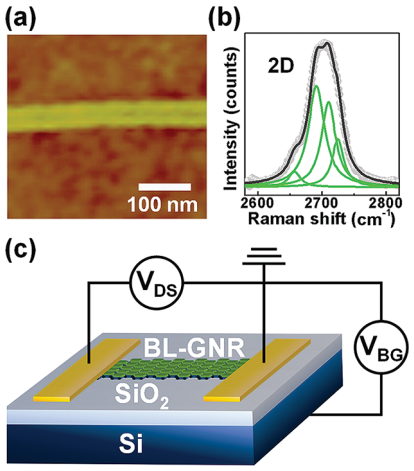

Figure 1. (a) AFM image of a 50 nm wide BL-GNR formed using a nanowire mask. (b) Raman spectrum of the bilayer graphene prior to the formation of the BL-GNR. The deconvolution of the 2D Raman peak to four Lorentzians confirms the A−B Bernal stacking order. (b) Schematic of the measurement setup. The source-drain contacts are Ti/Au, the thickness of the SiO_2 is 300 nm, and the degenerately doped (>2 × 10^{19} cm^{-3}) silicon substrate is used as the back gate. A frequency of ∼10 Hz and an AC voltage of δV_{DS} = 250 μV is used for the lock-in measurements.

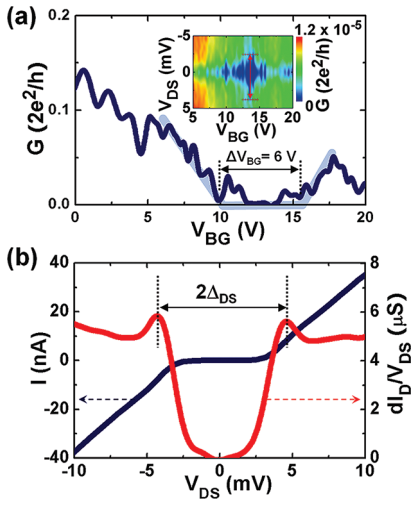

Figure 2. Gap-like features in BL-GNRs. (a) Conductance (G) dependence on the back-gate (V_{BG}) modulation at source-drain bias of $V_{DS} \approx 0$ V. Within V_{BG} = 10−16 V (ΔV_{BG} = 6 V), G is strongly suppressed with repeatable resonance peaks. The corresponding transport gap is ΔE_F = 87 meV. Inset: G *versus* V_{BG} and V_{DS}. (b) Current (I_D) and the differential conductance (dI_D/dV_{DS}) dependence on V_{DS} at V_{BG} = 13.5 V (the dashed line in the inset of panel a). The source-drain gap (Δ_{DS} = 4.4 meV) is half the voltage distance between the two peaks on the dI_D/dV_{DS}−V_{DS} curve.

gap and the field-induced energy gap, which suggests that the observed insulating state represents the transport gap induced by the disorders (*e.g.*, charge impurities and/or edge states) present along the nanoribbon. A gap-like feature can also be seen from the source-drain bias direction. The I_D−V_{DS} curve and the corresponding differential conductance (dI_D/dV_{DS}) at V_{BG} = 13.5 V (dashed line in Figure 2a inset) are plotted in Figure 2b. We extract the source-drain gap of $\Delta_{DS} \sim 4.4$ meV from the peak-to-peak distance on the dI_D/dV_{DS}−V_{DS} curve.

The disorder-induced gap features can be explained by two theoretical models: the quantum dot model[9,10] and the Anderson localization theory.[24,25] In order to clarify the origin of the disorder-induced gap in our BL-GNR, we precisely analyze the resonance peaks observed within the transport gap. As shown in Figure 3a, we observe periodic Coulomb diamonds, which is unlikely to result from the resonance between localized states[9] but is rather a strong indication of the quantum dot nature. The quantum dots in SL-GNRs are known to be formed by the surface potential fluctuation induced from disorders (charge impurities and/or edge roughness).[9,10,26] The existence and observation of both uncontrollable edge configurations[27] and charge impurities in bilayer graphene[28] makes us believe that the disordered surface potential is accountable for the Coulomb blockade behavior in our BL-GNR.

In the BL-GNR shown here, the periodic Coulomb blockade oscillations exclude the picture of a multidot system consisting of various dot sizes, although multidot behaviors are detected in other BL-GNR samples (see Supporting Information). In a multidot configuration, if the dots are exactly identical in size and potential profile, we would observe the same periodicity. This is because for each dot a slight difference in size and potential would lead to different charging energies (size) and S/D barriers (potential profile) and cause peak splitting upon gate modulation and/or temperature increase. However, the chance of having identical dots along the width and/or along the channel is extremely low. Thus, we believe that the data represent a single dot configuration. This can further be confirmed by measuring the temperature dependence of the oscillation peaks (Figure 3b).[29−31] As the temperature is decreased, no splitting is observed in the periodic conductance peaks, but only a parallel shift of the peak positions occurs. The peaks become sharper with decreasing temperature as the thermal broadening of the carrier distribution function reduces. This corroborates the fact that our BL-GNR is operating in a single quantum dot regime within the measured V_{BG} range and further allows us to estimate the size of the quantum dot as described below.

According to the classical Coulomb blockade theory, the diameter of a disk-shaped quantum dot can be determined by $d = e^2/(4\varepsilon\varepsilon_r E_C)$, where E_C is the charging energy of the quantum dot, ε is the permittivity of vacuum, and ε_r (=$(\varepsilon_{air} + \varepsilon_{SiO_2})/2$) is the relative permittivity of the surrounding dielectrics. On the basis of this model, the dot diameter is estimated to be ∼1 μm, which is larger than our BL-GNR dimensions (50 nm × 1.1 μm). The overestimation of the dot size is a result of neglecting the fringing effect[6,23] and the scaling of energy gaps (∼1/w)[10,32] in the quasi-one-dimensional BL-GNR geometry. Thus, we alternatively calculate the

TABLE 1. Comparison of the Band Structure, Energy Gaps, Transport Gaps, Carrier and Potential Fluctuation and Quantum Dot Size between SLG (SL-GNR) and BLG (BL-GNR) (Values Are Taken from Various Literatures and Our Current Work)

	dispersion relation near E_F	confinement gap	field-induced gap	carrier and potential fluctuation (experiment)[a]	carrier and potential fluctuation (theory)[a]	transport gap	quantum dot size
SLG	$E = \hbar k v_F$ ($v_F \sim 10^6$ m/s)[45]	$\Delta E \sim \hbar v_F/w$ (~6.6 meV, w ~50 nm)[22]	N/A	$\Delta n \sim 2.3 \times 10^{11}$ cm^{-2} (ΔE_d ~50 meV)[46]	$\Delta n \sim 1.2 \times 10^{11}$ cm^{-2} ΔE_d~36 meV (at $n_{imp} \sim 10^{11}$ cm^{-2})[37]	100—200 meV (w ~50 nm)[8] >200 meV (w ~30 nm)[9,47]	7850 nm^2 (w ~30 nm)[10] 3000 nm^2 (w ~30 nm)[9]
BLG	$E = \hbar^2k^2/2\,m^*$ (m^* ~0.054m_0)[11]	$\Delta E \sim \pi^2\hbar^2/m^*w^2$ (~5.6 meV, w ~50 nm)[b]	2 meV ($E \approx 0.02$ V/nm)[14]	$\Delta n \sim 3.8 \times 10^{11}$ cm^{-2} (ΔE_d ~20 meV)[28]	$\Delta n \sim 5.5 \times 10^{11}$ cm^{-2} ΔE_d ~29 meV (at $n_{imp} \sim 10^{11}$ cm^{-2})[37]	87 meV (w ~50 nm)[b]	12150—14000 nm^2 (w ~50 nm)[c]

[a] The Δn is the standard deviation of the carrier density fluctuation; ΔE_d is the corresponding surface potential fluctuation, and n_{imp} is the charge impurity concentration. Although ΔE_d is smaller in BLG due to the screening effects, BLGs have a wider distribution function of the carrier concentration fluctuation (larger Δn) than SLG because of the difference in dispersion relation.[37] [b] Estimated value. [c] Experimental results.

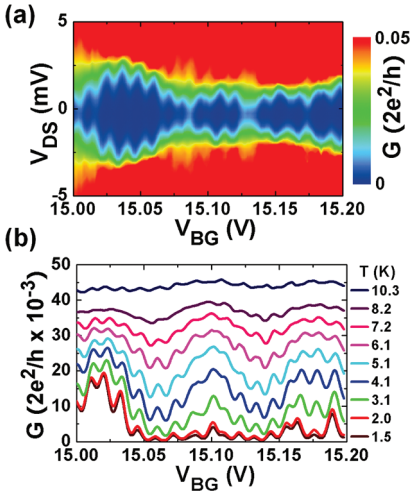

Figure 3. (a) Conductance *versus* V_{BG} and V_{DS}. The periodic Coulomb diamond indicates the quantum dot nature of the BL-GNR. (b) Periodic Coulomb oscillation peaks at different temperatures. With decreasing temperature, the peaks do not split, but shift parallel. The peaks become sharper at lower temperature because the thermal broadening reduces. This indicates that the BL-GNR is operating in the single dot regime within the measured V_{BG} range.

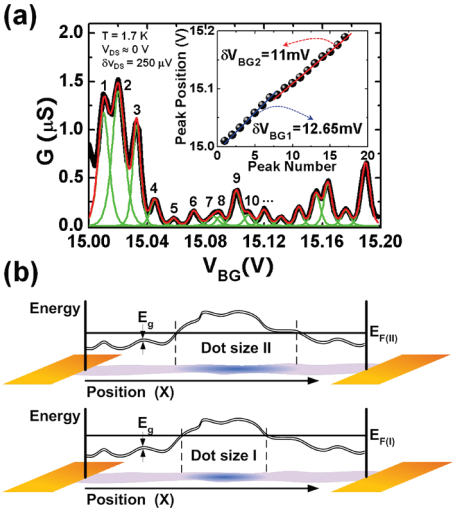

Figure 4. (a) Periodic Coulomb oscillation peaks. Every single peak is fitted (green lines) by the equation $G \sim \cosh^{-2}[e\alpha_{BG}(V - V_{peak})/2.5k_BT_{e(th)}]$, where the sum (red line) of all peaks matches the measurement data (black line) very well. Inset: the peak positions *versus* the peak numbers. Two different oscillation periods (δV_{BG1} = 12.65 mV, δV_{BG2} = 11.1 mV) are extracted through linear fitting, which corresponds to two different quantum dot sizes: 12 150 nm^2 (50 nm × 243 nm) and 14 000 nm^2 (50 nm × 280 nm). (b) Illustration of the change in quantum dot size. Upon modulation of the E_F by V_{BG}, the quantum dot becomes larger with smaller peak spacing δV_{BG2} at $E_{F(II)}$ compared to that at $E_{F(I)}$. (E_g is the combination of the confinement gap and the field-induced gap.)

capacitance per unit area ($\hat{C}_{BG}$) that includes the fringing effect (see Supporting Information) from our 50 nm wide BL-GNR on 300 nm SiO_2 ($\varepsilon_{SiO_2} \approx 3.9$). We then plot all 17 peaks (Figure 4a) as the function of peak numbers and extract two peak spacing values ($\delta V_{BG1} \sim 12.65$ mV, $\delta V_{BG2} \sim 11$ mV), each corresponding to a back-gate capacitance value ($C_{BG1} = 1.26 \times 10^{-17}$ F, $C_{BG2} = 1.45 \times 10^{-17}$ F). To obtain the quantum dot size, we divide $C_{BG1,2}$ by $\hat{C}_{BG}$ and find a 15% increase of the dot size from 12 150 nm^2 (50 nm × 243 nm) to 14 000 nm^2 (50 nm × 280 nm) upon increasing the back-gate voltage. This effect can be explained as illustrated in Figure 4b. The increase of the back-gate bias not only increases the number of electrons in the quantum dot but also gradually moves up the Fermi level (E_F) relative to the surface potential. When E_F is located at position I (bottom), the quantum dot size is relatively small and results in a large δV_{BG1}. When E_F moves to position II (top), the quantum dot becomes larger with a smaller δV_{BG2}.

In a Coulomb blockade system, another important parameter is the effective electron temperature, which represents the stability of the potential profile under thermal fluctuations and energy perturbations. We first examine the effect of thermal broadening from the line width of Coulomb oscillation peaks at $V_{DS} \approx 0$ V. We fit the peaks with the equation $G \sim \cosh^{-2}(e\alpha_{BG}(V - V_{peak})/2.5k_BT_{e(th)})$,[33] where $\alpha_{BG} = C_{BG}/C_{DOT}$ is the gate

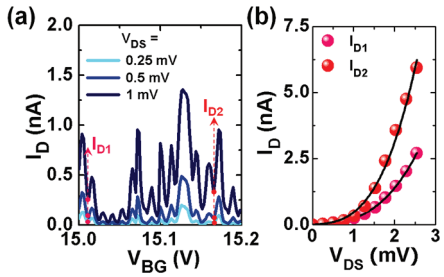

Figure 5. (a) Current *versus* V_{BG} at various V_{DS}. The valley current at the Coulomb blockade state increases with V_{DS}. The arrows indicate the Coulomb blockade state shown in panel b. (b) Valley current depending on V_{DS}. The effective electron temperature of $T_{e(ex)} < 2$K is obtained, which is nearly identical to the measurement temperature (1.7 K). This represents that the potential profile of the source/drain barriers remains stable under energy perturbations from external bias.

modulation factor, V_{peak} is the peak position, and $T_{e(th)}$ is the effective electron temperature relevant to thermal fluctuations. The extracted $T_{e(th)} = 2.1 \pm 0.5$ K is nearly identical to the measurement temperature (1.7 K), which implies that there is no considerable excess energy from extrinsic sources.

The excess energy, however, can arise when external electric fields are applied, particularly, from a source-drain bias.[34−36] This phenomenon can be characterized by co-tunneling events, which is associated with the valley current at the Coulomb blockade state. As shown in Figure 5a, the valley current increases with V_{DS}. The V_{DS} dependence of the valley current can be derived by $I_D = aG_SG_D[(eV_{DS})^2 + (2\pi k_B T_{e(ex)})]V_{DS}$,[34,35] where a is the proportional factor, G_S and G_D are the source and drain conductance, and $T_{e(ex)}$ is the effective electron temperature relevant to excess energies. By fitting the valley current with the above equation (Figure 5b), we obtain $T_{e(ex)} < 2$K, which is close to the measurement temperature (1.7 K), indicating the stability of the potential profile. Since the acoustic phonon scattering is negligible at $T = 1.7$ K, the slight discrepancy may be ascribed to electron−electron interactions.

Finally, we discuss several possible distinct properties of quantum dots in BL-GNRs compared to those of SL-GNRs, even though the potential fluctuations are responsible for both cases.[9,32] According to theoretical and experimental studies, bilayer graphene has a broader distribution function of the carrier concentration at the charge neutrality point for the same amount of charge impurities than that of single-layer graphene (Table 1).[28,37,38] This assists a single dot formation along a wide and long BL-GNR. In addition, the electric-field-induced energy gap may further increase the tunnel resistance[11] and promote quantum dot formation in BL-GNRs compared to SL-GNRs.

CONCLUSION

In conclusion, we studied the transport properties of BL-GNRs fabricated using nanowire etching masks. The Coulomb diamonds inside the transport gap reveal the quantum dot nature of the BL-GNR. The origin of the quantum dot is attributed to the disordered surface potential induced by charge impurities and/or edge roughness present along the nanoribbon. By extracting the effective temperatures related to thermal broadening and excess energies, we find that the potential profile forming the quantum dot in BL-GNRs is stable under thermal fluctuations and energy perturbations. Our results lead to the understanding that, for the potential use of BL-GNRs, the disordered surface potential fluctuations need to be reduced either by eliminating the charge impurities through the usage of suspended structures,[39] a hexagonal BN sacrificial layer, and high-κ dielectrics[40,41] or by minimizing the edge roughness utilizing a fabrication scheme with controlled edge roughness.[4,42] Alternatively, the stability of the potential profile can be exploited by fabricating local top gates for SET devices.

MATERIALS AND METHODS

Fabrication Method. Bilayer graphene samples were prepared by mechanical exfoliation on 300 nm silicon dioxide[1] thermally grown on a highly doped silicon substrate and characterized through Raman spectroscopy to determine the number of layers and the AB Bernal stacking order.[43] To form nanoribbons, silicon nanowires were mechanically transferred onto bilayer graphene samples[3,44] and used as etching masks. Uncovered graphene areas were etched away by oxygen plasma at 50 W for 10 s, which produced BL-GNRs with various widths. The silicon nanowire masks were then removed by ultrasonication, and Ti/Au source-drain contacts were deposited by electron-beam lithography.

Electrical Measurements. All measurements were conducted using a standard low-frequency lock-in technique ($f \sim 10$ Hz, $V_{AC} = 250\ \mu$V) at a temperature of 1.7 K (unless stated otherwise).

Acknowledgment. The authors would like to thank Dr. David Goldhaber-Gordon for fruitful discussions. This work was supported by the Focus Center Research Program (FCRP)−Functional Engineered Nano Architectonics (FENA) and the NSF IGERT Materials Creation Training Program Grant DGE-11443.

Supporting Information Available: Calculation method of the graphene nanoribbon's capacitance, the quantum dot size, and multidot behaviors in BL-GNRs. This material is available free of charge *via* the Internet at http://pubs.acs.org.

Note Added after ASAP Publication: This paper was published on October 23, 2011 with an error in the Results and Discussion section. The corrected version was reposted on November 22, 2011.

REFERENCES AND NOTES

1. Novoselov, K. S.; Geim, A. K.; Morozov, S. V.; Jiang, D.; Zhang, Y.; Dubonos, S. V.; Grigorieva, I. V.; Firsov, A. A. Electric Field Effect in Atomically Thin Carbon Films. *Science* **2004**, *306*, 666–669.
2. Han, M. Y.; Ozyilmaz, B.; Zhang, Y.; Kim, P. Energy Band-Gap Engineering of Graphene Nanoribbons. *Phys. Rev. Lett.* **2007**, *98*, 206805-4.

3. Bai, J.; Duan, X.; Huang, Y. Rational Fabrication of Graphene Nanoribbons Using a Nanowire Etch Mask. *Nano Lett.* **2009**, *9*, 2083–2087.
4. Li, X.; Wang, X.; Zhang, L.; Lee, S.; Dai, H. Chemically Derived, Ultrasmooth Graphene Nanoribbon Semiconductors. *Science* **2008**, *319*, 1229–1232.
5. Kosynkin, D. V.; Higginbotham, A. L.; Sinitskii, A.; Lomeda, J. R.; Dimiev, A.; Price, B. K.; Tour, J. M. Longitudinal Unzipping of Carbon Nanotubes To Form Graphene Nanoribbons. *Nature* **2009**, *458*, 872–876.
6. Lin, Y.-M.; Perebeinos, V.; Chen, Z.; Avouris, P. Electrical Observation of Subband Formation in Graphene Nanoribbons. *Phys. Rev. B* **2008**, *78*, 161409.
7. Xu, G.; Torres, C. M.; Song, E. B.; Tang, J.; Bai, J.; Duan, X.; Zhang, Y.; Wang, K. L. Enhanced Conductance Fluctuation by Quantum Confinement Effect in Graphene Nanoribbons. *Nano Lett.* **2010**, *10*, 4590–4594.
8. Han, M. Y.; Brant, J. C.; Kim, P. Electron Transport in Disordered Graphene Nanoribbons. *Phys. Rev. Lett.* **2010**, *104*, 056801.
9. Gallagher, P.; Todd, K.; Goldhaber-Gordon, D. Disorder-Induced Gap Behavior in Graphene Nanoribbons. *Phys. Rev. B* **2010**, *81*, 115409.
10. Stampfer, C.; Guttinger, J.; Hellmuller, S.; Molitor, F.; Ensslin, K.; Ihn, T. Energy Gaps in Etched Graphene Nanoribbons. *Phys. Rev. Lett.* **2009**, *102*, 056403.
11. McCann, E.; Abergel, D. S. L.; Fal'ko, V. I. Electrons in Bilayer Graphene. *Solid State Commun.* **2007**, *143*, 110–115.
12. Min, H.; Sahu, B.; Banerjee, S. K.; MacDonald, A. H. Ab Initio Theory of Gate Induced Gaps in Graphene Bilayers. *Phys. Rev. B* **2007**, *75*, 155115-7.
13. Oostinga, J. B.; Heersche, H. B.; Liu, X.; Morpurgo, A. F.; Vandersypen, L. M. K. Gate-Induced Insulating State in Bilayer Graphene Devices. *Nat. Mater.* **2008**, *7*, 151–157.
14. Zhang, Y.; Tang, T.-T.; Girit, C.; Hao, Z.; Martin, M. C.; Zettl, A.; Crommie, M. F.; Shen, Y. R.; Wang, F. Direct Observation of a Widely Tunable Bandgap in Bilayer Graphene. *Nature* **2009**, *459*, 820–823.
15. Katsnelson, M. I.; Novoselov, K. S.; Geim, A. K. Chiral Tunnelling and the Klein Paradox in Graphene. *Nat. Phys.* **2006**, *2*, 620–625.
16. Wright, A. R.; Cao, J. C.; Zhang, C. Enhanced Optical Conductivity of Bilayer Graphene Nanoribbons in the Terahertz Regime. *Phys. Rev. Lett.* **2009**, *103*, 207401.
17. Liu, J.; Wang, B.; Ma, Z.; Zhang, C. Two-Color Terahertz Response in Bilayer Graphene Nanoribbons with Spin–Orbit Coupling. *Appl. Phys. Lett.* **2011**, *98*, 061107.
18. Sahu, B.; Min, H.; MacDonald, A. H.; Banerjee, S. K. Energy Gaps, Magnetism, and Electric-Field Effects in Bilayer Graphene Nanoribbons. *Phys. Rev. B* **2008**, *78*, 045404.
19. Kim, G.; Jhi, S.-H. Spin-Polarized Energy-Gap Opening in Asymmetric Bilayer Graphene Nanoribbons. *Appl. Phys. Lett.* **2010**, *97*, 263114.
20. Guo, Y.; Guo, W.; Chen, C. Semiconducting to Half-Metallic to Metallic Transition on Spin-Resolved Zigzag Bilayer Graphene Nanoribbons. *J. Phys. Chem. C* **2010**, *114*, 13098–13105.
21. Li, X.; Zhang, Z.; Xiao, D. Pseudospin Valve in Bilayer Graphene Nanoribbons. *Phys. Rev. B* **2010**, *81*, 195402.
22. Ponomarenko, L. A.; Schedin, F.; Katsnelson, M. I.; Yang, R.; Hill, E. W.; Novoselov, K. S.; Geim, A. K. Chaotic Dirac Billiard in Graphene Quantum Dots. *Science* **2008**, *320*, 356–358.
23. Shylau, A. A.; Klstrokos, J. W.; Zozoulenko, I. V. Capacitance of Graphene Nanoribbons. *Phys. Rev. B* **2009**, *80*, 205402.
24. Evaldsson, M.; Zozoulenko, I. V.; Xu, H.; Heinzel, T. Edge-Disorder-Induced Anderson Localization and Conduction Gap in Graphene Nanoribbons. *Phys. Rev. B* **2008**, *78*, 161407.
25. Mucciolo, E. R.; Castro Neto, A. H.; Lewenkopf, C. H. Conductance Quantization and Transport Gaps in Disordered Graphene Nanoribbons. *Phys. Rev. B* **2009**, *79*, 075407.
26. Sols, F.; Guinea, F.; Neto, A. H. C. Coulomb Blockade in Graphene Nanoribbons. *Phys. Rev. Lett.* **2007**, *99*, 166803.
27. Xu, G.; Torres, J. C. M.; Bai, J.; Tang, J.; Yu, T.; Huang, Y.; Duan, X.; Zhang, Y.; Wang, K. L. Linewidth Roughness in Nanowire-Mask-Based Graphene Nanoribbons. *Appl. Phys. Lett.* **2011**, *98*, 243118.
28. Deshpande, A.; Bao, W.; Zhao, Z.; Lau, C. N.; LeRoy, B. J. Mapping the Dirac Point in Gated Bilayer Graphene. *Appl. Phys. Lett.* **2009**, *95*, 243502.
29. Ruzin, I. M.; Chandrasekhar, V.; Levin, E. I.; Glazman, L. I. Stochastic Coulomb Blockade in a Double-Dot System. *Phys. Rev. B* **1992**, *45*, 13469.
30. Ishikuro, H.; Fujii, T.; Saraya, T.; Hashiguchi, G.; Hiramoto, T.; Ikoma, T. Coulomb Blockade Oscillations at Room Temperature in a Si Quantum Wire Metal-Oxide-Semiconductor Field-Effect Transistor Fabricated by Anisotropic Etching on a Silicon-on-Insulator Substrate. *Appl. Phys. Lett.* **1996**, *68*, 3585–3587.
31. Ishikuro, H.; Hiramoto, T. Quantum Mechanical Effects in the Silicon Quantum Dot in a Single-Electron Transistor. *Appl. Phys. Lett.* **1997**, *71*, 3691–3693.
32. Molitor, F.; Stampfer, C.; Guttinger, J.; Jacobsen, A.; Ihn, T.; Ensslin, K. Energy and Transport Gaps in Etched Graphene Nanoribbons. *Semicond. Sci. Technol.* **2010**, *25*, 034002.
33. Kouwenhoven, L. P.; Marcus, C. M.; McEuen, P. L.; Tarucha, S.; Westervelt, R. M.; Wingreen, N. S. In *Electron Transport in Quantum Dots*, Proceedings of the NATO Advanced Study Institute on Mesoscopic Electron Transport; Sohn, L. L., Kouwenhoven, L. P.; Schon, G., Eds.; Kluwer Academic Publishers: Dordrecht, The Netherlands, 1997; pp 105–214.
34. Lee, S.; Hiramoto, T. Strong Dependence of Tunneling Transport Properties on Overdriving Voltage for Room-Temperature-Operating Single Electron/Hole Transistors Formed with Ultranarrow [100] Silicon Nanowire Channel. *Appl. Phys. Lett.* **2008**, *93*, 043508.
35. Takahashi, Y.; Horiguchi, S.; Fujiwara, A.; Murase, K. Cotunneling Current in Very Small Si Single-Electron Transistors. *Phys. B* **1996**, *227*, 105–108.
36. De Franceschi, S.; Sasaki, S.; Elzerman, J. M.; van der Wiel, W. G.; Tarucha, S.; Kouwenhoven, L. P. Electron Cotunneling in a Semiconductor Quantum Dot. *Phys. Rev. Lett.* **2001**, *86*, 878.
37. Das Sarma, S.; Hwang, E. H.; Rossi, E. Theory of Carrier Transport in Bilayer Graphene. *Phys. Rev. B* **2010**, *81*, 161407.
38. Hwang, E. H.; Das Sarma, S. Insulating Behavior in Metallic Bilayer Graphene: Interplay between Density Inhomogeneity and Temperature. *Phys. Rev. B* **2010**, *82*, 081409.
39. Bolotin, K. I.; Sikes, K. J.; Jiang, Z.; Klima, M.; Fudenberg, G.; Hone, J.; Kim, P.; Stormer, H. L. Ultrahigh Electron Mobility in Suspended Graphene. *Solid State Commun.* **2008**, *146*, 351–355.
40. Adam, S.; Hwang, E. H.; Galitski, V. M.; Das Sarma, S. A Self-Consistent Theory for Graphene Transport. *Proc. Natl. Acad. Sci. U.S.A.* **2007**, *104*, 18392–18397.
41. Chen, F.; Xia, J.; Ferry, D. K.; Tao, N. Dielectric Screening Enhanced Performance in Graphene FET. *Nano Lett.* **2009**, *9*, 2571–2574.
42. Jiao, L.; Zhang, L.; Wang, X.; Diankov, G.; Dai, H. Narrow Graphene Nanoribbons from Carbon Nanotubes. *Nature* **2009**, *458*, 877–880.
43. Ferrari, A. C.; Meyer, J. C.; Scardaci, V.; Casiraghi, C.; Lazzeri, M.; Mauri, F.; Piscanec, S.; Jiang, D.; Novoselov, K. S.; Roth, S.; *et al.* Raman Spectrum of Graphene and Graphene Layers. *Phys. Rev. Lett.* **2006**, *97*, 187401-4.
44. Bai, J.; Cheng, R.; Xiu, F.; Liao, L.; Wang, M.; Shailos, A.; Wang, K. L.; Huang, Y.; Duan, X. Very Large Magnetoresistance in Graphene Nanoribbons. *Nat. Nanotechnol.* **2010**, *5*, 655–659.
45. Neto, A. H. C.; Guinea, F.; Peres, N. M. R.; Novoselov, K. S.; Geim, A. K. The Electronic Properties of Graphene. *Rev. Mod. Phys.* **2009**, *81*, 109–154.
46. Martin, J.; Akerman, N.; Ulbricht, G.; Lohmann, T.; Smet, J. H.; von Klitzing, K.; Yacoby, A. Observation of Electron-Hole Puddles in Graphene Using a Scanning Single-Electron Transistor. *Nat. Phys.* **2008**, *4*, 144–148.
47. Molitor, F.; Jacobsen, A.; Stampfer, C.; Güttinger, J.; Ihn, T.; Ensslin, K. Transport Gap in Side-Gated Graphene Constrictions. *Phys. Rev. B* **2009**, *79*, 075426.